# Optimizing quantum gates within decoherence-free subspaces

Xiaoxiao Hu,[1] Feihao Zhang,[2] Yansong Li,[1] and Guilu Long[1,2,3,4,*]

[1]*State Key Laboratory of Low-Dimensional Quantum Physics and Department of Physics, Tsinghua University, Beijing 100084, China*

[2]*Beijing Academy of Quantum Information Sciences, Beijing 100193, China*

[3]*Frontier Science Center for Quantum Information, Beijing 100084, China*

[4]*Beijing National Research Center for Information Science and Technology, Beijing 100084, China*

(Received 28 May 2021; accepted 30 November 2021; published 15 December 2021)

A scheme for optimizing quantum gates in quantum computation on decoherence-free subspaces using optimal control theory is presented. Compared with the previous scheme, this scheme possesses the following properties: (i) efficiency in finding control sequences, specifically in a system without controllable exchange interaction where the previous method is difficult to handle; (ii) robustness against control errors; and (iii) showing better performance than the robust GRAPE method under stochastic noise. As an application, we work out the control sequences for the NOT, quantum phase, and CNOT gates.

DOI: 10.1103/PhysRevA.104.062612

## I. INTRODUCTION

The key task in implementing quantum information processing is to drive the system to evolve in the way we want [1,2]. Two challenges prevent the quantum system from evolving into the target state: the decoherence due to the uncontrolled interaction between the system and the environment, and the error produced in the control process [3]. For instance, in a spin-qubit system, the thermal distribution of the environmental spins may cause a quasistatic noise field on the system spins [4]. The coherent evolution of the coupled nearby environmental spins is another possible source and causes a stochastic fluctuating noise. Besides the decoherence caused by the environment, the control error would, unwanted, change the quantum evolution path. Experimentally, those errors can come from the linear or nonlinear distortion of input control sequences by the classical electronic hardware [5,6]. There are several techniques to overcome those obstacles, i.e., decoherence-free subspaces (DFSs) [7–20]; quantum optimal control theory (OCT) [21,22], including the gradient ascent pulse engineering (GRAPE) method [23–33]; and noise cancellation [6,34].

Encoding states in decoherence-free subspaces is an effective way to protect quantum information from decoherence. The basic idea of DFS is to make use of the algebraic symmetry structure of the interaction between the system and the environment to store quantum information inside a subspace where the system undergoes a unitary evolution [10]. A more detailed analysis of DFS presents us with necessary and sufficient conditions for dynamically stable DFS [35]. The theory of DFS is extended to time-dependent DFS, where the basis of DFS is varying with time [36]. A method of implementing universal quantum gates in the DFS has been proposed in Ref. [11] and has been demonstrated in several physical quantum systems [12,16,20,37]. However, this method poses stringent criteria on the control Hamiltonian of the system. Thus, these methods have difficulty in finding proper control sequences to realize an arbitrary quantum gate if the system does not satisfy the criteria.

The quantum optimal control theory has been used in efforts to engineer quantum systems. Many efficient and robust quantum control techniques have been discovered in recent years [22]. A widely used numerical method is GRAPE, as one of the optimal control designs. The method combines the numerical optimization method with quantum control, so as to search the high-fidelity control scheme. The GRAPE method has been proven to improve the robustness against linear and nonlinear distortions [5,38–40]. And by multiobjective optimization, it also possesses robustness against quasistatic environmental noise [32]. However, it has difficulty dealing with stochastic environmental noise.

The quantum OCT offers a flexible framework for designing a quantum control process. Useful applications in this field include optimal control combined dynamical decoupling [41], closed-loop optimal control using experimental feedback [42], realization of adiabatic evolution [43], holonomic gates [44], etc. In this work, we propose a method by combining the idea of DFS with OCT. We quantify the DFS conditions in the form of a loss function of the control sequences. As a development of OCT, we derive the objective function by combining the loss function with the control fidelity. Furthermore, the control errors can be suppressed by optimizing averaged objective function as in the robust GRAPE method. Our method protects the quantum information process against stochastic noise by constraining the system to evolve within a DFS for most of the time during the control process and remove the restriction on the control Hamiltonian [11]. Another advantage is that the algorithm can automatically give the corresponding control sequences of the target quantum gate. We numerically realize the NOT gate, the quantum phase gate, and the CNOT gate and demonstrate the robustness of our method against

*gllong@mail.tsinghua.edu.cn

 

control errors and quasistatic environmental noises. Moreover, to show our method possesses robustness against stochastic noises, we also compare our method with the robust GRAPE with different noises which have different correlation times. The simulations show that our method maintains high fidelity during the whole regime.

## II. THEORY OF QUANTUM GATE PROTECTED BY DFS

### A. System and control Hamiltonian

We consider a quantum system $S$ made of qubits. The system is coupled to an environmental bath $B$ and the total Hamiltonian is given by

$$H(t) = [H_0 + H_C(t)] \otimes \mathbb{I}_B + \mathbb{I}_S \otimes H_B + H_I, \tag{1}$$

where $H_0$ ($H_B$) is the system (bath) Hamiltonian, $H_C(t)$ is the time-dependent control Hamiltonian acting on the system, $\mathbb{I}_S$ ($\mathbb{I}_B$) is the identity operator on the system (bath), and $H_I$ is the system-environment interaction Hamiltonian.

Generally, the control Hamiltonian can be expressed as

$$H_C(t) = \sum_\alpha h_\alpha(t) H_\alpha, \tag{2}$$

where $H_\alpha$ is the $\alpha$th part of the control Hamiltonian, and $h_\alpha(t)$ is the corresponding time-dependent control field amplitude. Assume also that the interaction can be written as

$$H_I = \sum_\alpha S_\alpha \otimes B_\alpha, \tag{3}$$

where $S_\alpha$ ($B_\alpha$) acts solely on the system (bath). The evolution of the density matrix $\rho$ of an open system is given by the Markovian master equation [45]

$$\dot{\rho} = -i[H_S(t), \rho] + L_D[\rho], \tag{4}$$

where we neglect the *Lamb shift* Hamiltonian of the system, so the unitary evolution is given by the time-dependent system Hamiltonian $H_S(t) = H_0 + H_C(t)$. The decoherence of the system depends on

$$L_D[\rho] = \frac{1}{2} \sum_\alpha \gamma_\alpha ([S_\alpha \rho, S_\alpha^\dagger] + [S_\alpha, \rho S_\alpha^\dagger]), \tag{5}$$

where $\gamma_\alpha$ is coefficient of the diagonalized decoherence operator $\{S_\alpha\}$.

### B. DFS condition and the objective function

The condition for generic DFS was proposed in Ref. [11] by defining that the dissipative part of the Markovian master equation is zero. However, a further study has proven that the condition is neither sufficient nor necessary. A DFS $\tilde{\mathcal{H}}_{\rm DFS}$ is defined as a subspace of an open system with Hilbert space $\tilde{\mathcal{H}}$ such that all states $\rho(t)$ in the DFS fulfill $\partial_t {\rm Tr}[\rho^2(t)] = 0$, for $\forall t \geqslant 0$, with ${\rm Tr}[\rho^2(0)] = 1$ [35]. From this definition, it has been proven that the subspace $\tilde{\mathcal{H}}_{\rm DFS} = {\rm Span}\{|\psi_1\rangle, |\psi_2\rangle, \ldots |\psi_M\rangle\}$ is a DFS iff [35,36]

(i) $S_\alpha |\psi_j\rangle = c_\alpha |\psi_j\rangle$ $(j = 1, \ldots, M; \alpha = 1, \ldots, K)$;

(ii) $\tilde{\mathcal{H}}_{\rm DFS}$ is invariant under $H_{\rm eff} = H_{\rm S} + \frac{i}{2} \sum_\alpha \gamma_\alpha (c_\alpha^* S_\alpha - c_\alpha S_\alpha^\dagger)$.

The evolution of a system that satisfies the DFS conditions is given by

$$\dot{\rho} = -i[H_{\rm eff}, \rho]. \tag{6}$$

${\rm Tr}[\rho^2(0)] = 1$ means that the state of the system is pure for $t = 0$. It can be easily met because the state of the system is always initialized into a pure state in an experiment.

Condition (i) provides a criterion to find a DFS that every basis $\{|\psi_i\rangle\}$ of $\tilde{\mathcal{H}}_{\rm DFS}$ should be a common eigenstate of all $S_\alpha$. Let $\tilde{\mathcal{H}}_{\rm DFS^\perp}$ denote the orthogonal complement space of $\tilde{\mathcal{H}}_{\rm DFS}$ in $\tilde{\mathcal{H}}$ and be spanned by $\{|\phi_1\rangle, |\phi_2\rangle, \ldots |\phi_L\rangle\}$. The system's Hilbert space $\tilde{\mathcal{H}}$ is the direct sum of the two subspaces: $\tilde{\mathcal{H}} = \tilde{\mathcal{H}}_{\rm DFS} \oplus \tilde{\mathcal{H}}_{\rm DFS^\perp}$, and accordingly, the projective operator $\Pi$ on the system Hilbert space is the direct sum of projectors on $\tilde{\mathcal{H}}_{\rm DFS}$ and $\tilde{\mathcal{H}}_{\rm DFS^\perp}$: $\Pi = \Pi_{\rm DFS} \oplus \Pi_{\rm DFS^\perp}$.

Condition (ii) is the DFS preserving condition. It ensures that the system on $\tilde{\mathcal{H}}_{\rm DFS}$ driven by $H_{\rm eff}$ does not evolve out of the subspace during the total control time $\tau$. We rewrite the condition as

$$\langle \phi_i | U(t) | \psi_j \rangle = r_{ij}(t) = 0$$
$$(i = 1, \ldots, L; \quad j = 1, \ldots, M; \quad 0 \leqslant t \leqslant \tau), \tag{7}$$

where $U(t) = \mathcal{T} \exp[-i\hbar \int_0^t H_{\rm eff}(t')dt']$. In order to quantify this condition, we define a loss function $\Phi_1$,

$$\Phi_1 = \frac{1}{\tau} \int_0^\tau \sum_{ij} r_{ij}(t) r_{ij}^*(t) dt$$
$$= {\rm Tr}\left( \frac{1}{\tau} \int_0^\tau U(t) \Pi_{\rm DFS^\perp} U^\dagger(t) \Pi_{\rm DFS} dt \right) \geqslant 0. \tag{8}$$

Then Eq. (7) is equivalent to $\Phi_1 = 0$. So by minimizing $\Phi_1$, condition (iii) can be fulfilled.

Now we consider the task that the evolution of the system $U(\tau)$ approaches a target propagator $U_T$ on a DFS. The entanglement fidelity between the target gate and the evolution of the system is another quantity in optimization [46,47] and we define $\Phi_2$ as

$$\Phi_2 = \frac{|{\rm Tr}[U_T^\dagger U(\tau)]|^2}{{\rm Tr}(\Pi_{\rm DFS})^2}. \tag{9}$$

When $\Phi_2$ reaches its maximum after a control process, the evolution $U(\tau)$ acquires a maximum overlap with the target gate $U_T$ in the DFS.

Combining $\Phi_1$ and $\Phi_2$, we set the objective function $O(\{h_\alpha(k)\})$ as

$$O(\{h_\alpha(k)\}) = \Phi_2 - \lambda \cdot \Phi_1$$
$$= \frac{|{\rm Tr}[U_T^\dagger U(\tau)]|^2}{{\rm Tr}(\Pi_{\rm DFS})^2}$$
$$- \lambda \cdot {\rm Tr}\left( \frac{1}{\tau} \int_0^\tau U(t) \Pi_{\rm DFS^\perp} U(t)^\dagger \Pi_{\rm DFS} dt \right), \tag{10}$$

where $\lambda$ is a positive parameter. In practice, the total control time $\tau$ is discretized in $N$ equal steps of duration $\Delta t = \tau/N$, during which the control field amplitudes are constant. Denote $h_\alpha(k)$ as the amplitude of the $\alpha$th control Hamiltonian $H_\alpha$ during the $k$th step. Therefore, the control sequences $\{h_\alpha(k)\}$ that maximize the objective function $O(\{h_\alpha(k)\})$ will drive the

system to the target evolution while preserving the evolution within DFS for most of the time in the control process. The computing method for the integral in Eq. (10) is given in Appendix A.

### C. Robustness against control error

The control Hamiltonian given in Eq. (2) is only the ideal case. Errors from the quasistatic fluctuation of electronic devices contribute to the distortions of the control amplitudes [31]. The timescale of the linear deviation $\delta$ is much longer than our single control process, so we can take it as a random constant. The control Hamiltonian with errors can then be expressed as $H_C(t,\delta) = \sum_\alpha (1+\delta) h_\alpha(t) H_\alpha$. The previous work has shown that $\delta$ follows a Lorentzian distribution $p(\delta) = \gamma/\pi(\delta^2+\gamma^2)$, where $\gamma$ is the scale parameter of the half-width at half maximum of this distribution [31].

Denote $O(\{h_\alpha(k)\},\delta)$ as the corresponding objective function of control sequences for an error $\delta$. To suppress $\delta$, we optimize the average objective function defined as

$$\overline{O}(\{h_\alpha(k)\}) = \int d\delta\ p(\delta) O(\{h_\alpha(k)\},\delta). \tag{11}$$

In the practical implementation of the optimization, we discretize the continuous distribution function $p(\delta)$. Equation (11) turns into discrete summation:

$$\overline{O}(\{h_\alpha(k)\}) = \sum_\delta p(\delta) O(\{h_\alpha(k)\},\delta). \tag{12}$$

We use the algorithm described in Appendix B to optimize the control sequences.

## III. REALIZATION OF OPTIMIZED QUANTUM GATE WITH DFS IN QUANTUM COMPUTATION

Considering the example of the spin qubit system, we assume that all qubits are coupled to the same bath [48], which is known as a *collective model*. The interaction Hamiltonian can be expressed as

$$\begin{aligned} H_{SB} &= \sum_{i,\alpha} (\sigma_\alpha^i) \otimes B_\alpha = \sum_\alpha S_\alpha \otimes B_\alpha \\ &(i = 1,\ldots,N; \quad \alpha = I,X,Y,Z). \end{aligned} \tag{13}$$

It has been found that, for most of the quantum systems, the longitudinal relaxation time of qubits is several orders of magnitude longer than the transverse. So that the pure dephasing effect is a major influence on many quantum systems [17]. This implies that the spin-bath interaction can be written as

$$\begin{aligned} H_{SB} &= \sum_i \sigma_z^i \otimes B_z \\ &= S_z \otimes B_z. \end{aligned} \tag{14}$$

The following examples are considered as pure dephasing *collective model*s..

### A. NOT gate and quantum phase gate

To illustrate our method, we consider an example of two physical qubits in an NMR system [18]. The system Hamiltonian has the form

$$H_0 = \frac{\omega_0}{2}\left(\sigma_z^1 + \sigma_z^2\right) + \pi\left(\nu_1\sigma_z^1 + \nu_2\sigma_z^2 + J\sigma^1\cdot\sigma^2/2\right), \tag{15}$$

where $\omega_0$ is the Zeeman splitting, the frequency shift is $\Delta = \nu_2 - \nu_1 = -137.5$ Hz, and the $J$-coupling constant is $J = 5.7$ Hz. The control Hamiltonian, describing the interaction between the qubits and the applied radiofrequency (RF) field, is written as

$$H_C(t) = \Omega(t)\sum_{i=1}^{2}\left\{\cos[\omega_{\rm RF}t + \phi(t)]\sigma_x^i + \sin[\omega_{\rm RF}t + \phi(t)]\sigma_y^i\right\}, \tag{16}$$

where $\Omega(t)$ is the amplitude of the RF pulse, $\omega_{\rm RF}$ is the frequency of the RF pulse, and $\phi(t)$ is the phase. With $\omega_{\rm RF} = \omega_0 + \pi\nu_1$, we take the rotating frame $\hat{R}(t) = e^{-i(\frac{\omega_0}{2}+\pi\nu_1)(\sigma_z^1+\sigma_z^2)t}$. In the frame, the system Hamiltonian and the control Hamiltonian are expressed as

$$\begin{aligned} H_0 &= \pi\left(\Delta\sigma_z^2 + J\sigma^1\cdot\sigma^2\right), \\ H_C(t) &= \sum_{\alpha=x,y} h_\alpha(t)\left(\sigma_\alpha^1 + \sigma_\alpha^2\right), \end{aligned} \tag{17}$$

where $h_x(t) = \Omega(t)\cos\phi(t)$ and $h_y(t) = \Omega(t)\sin\phi(t)$.

We choose a DFS of the system spanned by $\{|01\rangle, |10\rangle\}$, where $|0\rangle$ and $|1\rangle$ are the eigenstates of the Pauli matrix $\sigma_z$, and encode the logical one qubit in the DFS as $\{|\tilde{0}\rangle = |01\rangle, |\tilde{1}\rangle = |10\rangle\}$. Note that $S_z|\psi\rangle = 0$ for all $|\psi\rangle$ in $\tilde{\mathcal{H}}_{\rm DFS}$. This implies that $\frac{i}{2}\sum_\alpha \gamma_\alpha(c_\alpha^* S_\alpha - c_\alpha S_\alpha^\dagger) = 0$; hence, $H_{\rm eff} = H_S(t) = H_0 + H_C(t)$.

The NOT gate $G_{\rm NOT}$ in basis of $\{|\tilde{0}\rangle, |\tilde{1}\rangle\}$ is expressed as

$$\begin{aligned} G_{\rm NOT} &= |\tilde{0}\rangle\langle\tilde{1}| + |\tilde{1}\rangle\langle\tilde{0}| \\ &= \begin{pmatrix} 0 & 0 & 0 & 0 \\ 0 & 0 & 1 & 0 \\ 0 & 1 & 0 & 0 \\ 0 & 0 & 0 & 0 \end{pmatrix}, \end{aligned} \tag{18}$$

and the phase gate $G_P$ is expressed as

$$\begin{aligned} G_P &= |\tilde{0}\rangle\langle\tilde{0}| + i|\tilde{1}\rangle\langle\tilde{1}| \\ &= \begin{pmatrix} 0 & 0 & 0 & 0 \\ 0 & 1 & 0 & 0 \\ 0 & 0 & i & 0 \\ 0 & 0 & 0 & 0 \end{pmatrix}. \end{aligned} \tag{19}$$

The control sequences are robust against control error by using the average objective function, Eq. (12). Rewrite the average objective function in the following discrete summation form:

$$\begin{aligned} \overline{O}(\{h_\alpha(k)\}) = \sum_\delta p(\delta)\Bigg\{ &\frac{1}{{\rm Tr}(\Pi_{\rm DFS})^2}|{\rm Tr}[U_{\rm T}U(N,\delta)]|^2 \\ &- \frac{\lambda}{N}\sum_{k=1}^{N} U(k,\delta)\Pi_{\rm DFS^\perp}U^\dagger(k,\delta)\Pi_{\rm DFS}\Bigg\}, \end{aligned} \tag{20}$$

where the evolution of the system is

$$U(k,\delta) = \prod_{j=k}^{1}\exp\left\{-i\frac{\tau}{N}\left(H_0 + \sum(1+\delta)h_\alpha(j)H_\alpha\right)\right\}. \tag{21}$$

We set $\tau = 20$ ms and $N = 100$. To guarantee the DFS conditions, we set $\lambda = 0.1$. The maximum intensity of the control sequences is set to be $1\pi$ kHz, and the discrete distribution is expressed as

$$p(\delta) = \begin{cases} 0.3, & \delta = -5\%, \\ 0.4, & \delta = 0\%, \\ 0.3, & \delta = 5\%. \end{cases} \tag{22}$$

The control sequences of $G_{\mathrm{NOT}}$ and $G_{\mathrm{P}}$ can be found by our method, by setting $U_{\mathrm{T}}$ to be $G_{\mathrm{NOT}}$ and $G_{\mathrm{P}}$, respectively. Then by maximizing the target function $\overline{O}(\{h_\alpha(k)\})$, we can optimize control sequences of the NOT gate and the phase gate, respectively. The wave forms of our control sequences are shown in Appendix D [Figs. 7(a) and 7(b) and Figs. 8(a) and 8(b)].

First, we test the performance of gates designed by our method in the presence of quasistatic environmental noise and a linear deviation of control amplitudes. The Hamiltonian we use to simulate the evolution of the system can be expressed as

$$H(t, \delta, \beta_z) = H_0 + (1 + \delta)H_C + S_z\beta_z, \tag{23}$$

where the control error amplitude is $\delta$, and $\beta_z$ is the environmental noise strength. We calculate the fidelities defined in Eq. (9) of the control sequence designed by our method. The results are shown in Figs. 1(a) and 2(a). For the purpose of comparison, we also gain the control sequences of the robust GRAPE [23]. Details are shown in Appendix C. The control sequences are shown in Appendix D [Figs. 7(c) and 7(d) and Figs. 8(c) and 8(d)]. The results are shown in Figs. 1(b) and . 2(b). The typical $T_2^*$ of the NMR system is about 500 ms, so $\beta_z$ is mostly distributed within $[-2, 2]$ Hz. The control error is mostly distributed in $[-0.5\%, 0.5\%]$ [31]. The fidelities of the NOT gate and the phase gate by both our method and robust GRAPE are above 0.9992 if $-2$ Hz $\leqslant \beta_z \leqslant 2$ Hz and $-0.5\% \leqslant \delta \leqslant 0.5\%$. The results imply that both our method and robust GRAPE satisfy requirements for experiment under quasistatic errors. Beyond quasistatic errors, our method is robust against stochastic noises which also play roles in the decoherence effect.

Stochastic noises widely exist in different quantum systems. For the NMR system, the stochastic noises come from a wide range of molecular motions. The timescales of noises depend on the motional mechanisms and run from fractions of a picosecond, through nanoseconds, milliseconds, to many seconds [4]. In order to test the performance of the control sequences under stochastic noises which have different correlation times, we employ a classical model [49,50]:

$$H_{SB} = S_z\beta(t), \tag{24}$$

where $\beta(t)$ is a Gaussian distributed random variable with $\langle\beta(t)\rangle = 0$ and $\sqrt{\langle\beta(t)^2\rangle} = 2.5$ Hz. For $\beta(t)$ with the noise correlation time $t_{\mathrm{cor}}$ [51], we simulate the noise by extracting the random number $\beta(i)$ from the Gaussian distribution as a constant noise during $[(i-1)t_{\mathrm{cor}}, it_{\mathrm{cor}}]$. $\tau/t_{\mathrm{cor}}$ are set to be integers. We calculate the fidelities with $\tau/t_{\mathrm{cor}}$ ranging from 1 to 100. The noise is static during the control process if $\tau/t_{\mathrm{cor}}$ is choosen to be 1, and the noise changes for every time step of the control sequences if $\tau/t_{\mathrm{cor}}$ be 100.

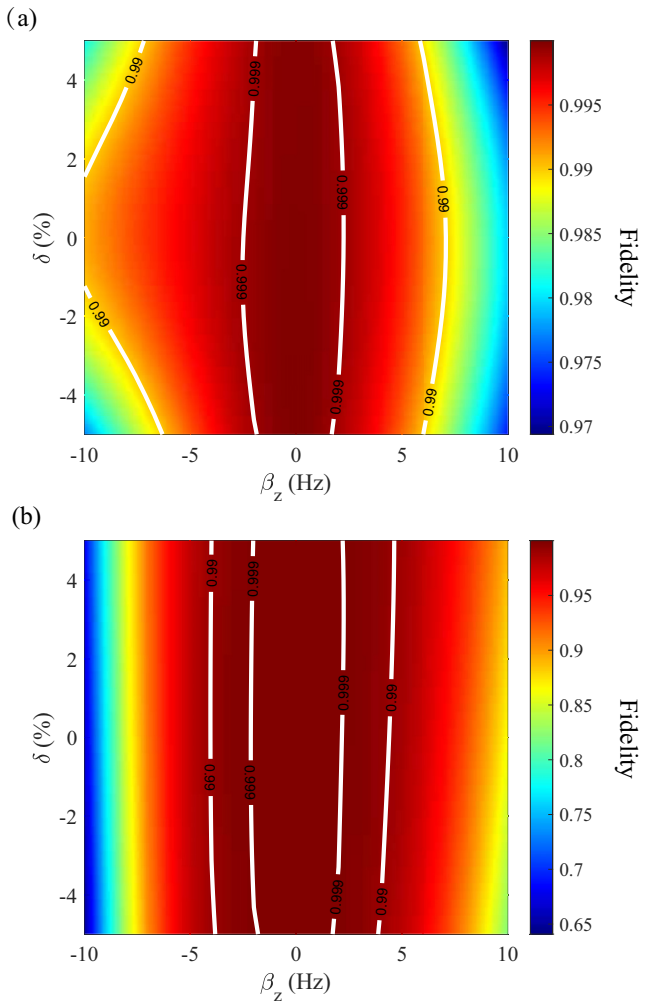


FIG. 1. The fidelities for the NOT gates searched by our method and robust GRAPE, in the presence of quasistatic environmental noise and the linear distortion. The $x$ axis represents the environmental noise strength, the $y$ axis represents the control error, and the fidelities for the gates are depicted in the color jets. (a) The fidelities for our method. (b) The fidelities for robust GRAPE.

Figures 3 and 4 show the fidelities of the two methods for the NOT gate and the phase gate, respectively. The fidelities of the control sequences for the NOT gate searched by our method are not less than 0.997 in noise with $\tau/t_{\mathrm{cor}}$ ranging from 1 to 100, and the fidelities for the phase gate are not less than 0.998. The fidelities of the gates by robust GRAPE collapse in noise with correlation time which lies in the intermediate regime.

From the comparisons of the two protocols in the above simulations, we demonstrate that our method has performance similar to that of robust GRAPE against quasistatic decoherence noises and quasistatic control errors. However, in the case of stochastic noise, our method works better than robust GRAPE.

### B. CNOT gate

We use four physical qubits in an NMR system [52] to implement the CNOT gate. The system Hamiltonian has the

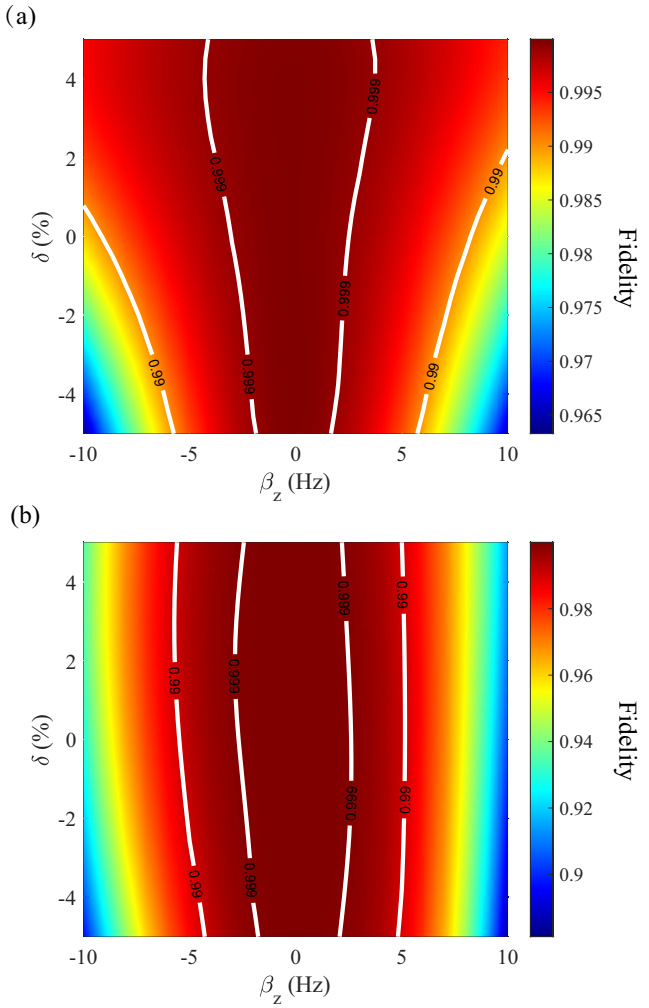


FIG. 2. The fidelities for phase gates searched by our method and robust GRAPE, in the presence of quasistatic environmental noise and linear distortion. The $x$ axis represents the environmental noise strength, the $y$ axis represents the control error, and the fidelities for the gates are depicted in the color jets. (a) The fidelities for our method. (b) The fidelities for robust GRAPE.

form

$$H_0 = \sum_{j=1}^{4}(\omega_0 - \pi\nu_j)\sigma_z^j + \sum_{j<k}^{4}\frac{\pi}{2}J_{jk}\sigma_z^j\sigma_z^k, \tag{25}$$

where $\omega_0$ is the Zeeman splitting and the chemical shifts $\nu_i$ and the $J$-coupling $J_{jk}$ are given by the diagonal and off-diagonal elements in Table I [52]. The control Hamiltonian is written as

$$H_C(t) = \Omega(t)\sum_{i=1}^{4}\{\cos[\omega_{\mathrm{RF}}t + \phi(t)]\sigma_x^i + \sin[\omega_{\mathrm{RF}}t + \phi(t)]\sigma_y^i\}. \tag{26}$$

Given $\omega_{\mathrm{RF}} = \omega_0$, the corresponding system Hamiltonian and the control Hamiltonian in the rotating frame $\hat{R}(t) = e^{-i\omega_0(\sigma_z^1+\sigma_z^2+\sigma_z^3+\sigma_z^4)t}$ are expressed as

$$H_0 = -\sum_{j=1}^{4}\pi\nu_j\sigma_z^j + \sum_{j<k}^{4}\frac{\pi}{2}J_{jk}\sigma_z^j\sigma_z^k,$$
$$H_C(t) = \sum_{\alpha=x,y}h_\alpha(t)\left(\sigma_\alpha^1 + \sigma_\alpha^2 + \sigma_\alpha^3 + \sigma_\alpha^4\right), \tag{27}$$

where $h_x(t) = \Omega(t)\cos\phi(t)$ and $h_y(t) = \Omega(t)\sin\phi(t)$.

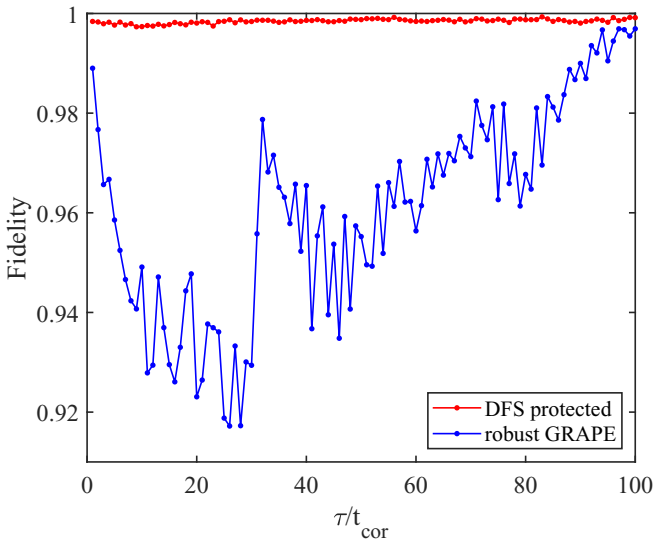


FIG. 3. The fidelities for NOT gates searched by our method and robust GRAPE, in stochastic noise of different correlation times. The red broken line shows the fidelities for our method, and the blue broken line shows the fidelities for robust GRAPE. The $x$ axis is the ratio of the control time $\tau$ and the correlation time of the noise $t_{\mathrm{cor}}$.

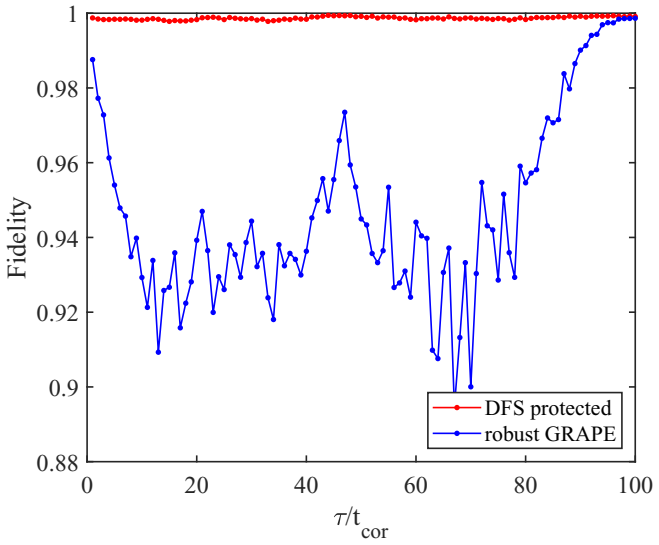


FIG. 4. The fidelities of phase gates searched by our method and robust GRAPE, in a stochastic noise of different correlation times. The red broken line shows our method, and the blue broken line shows robust GRAPE. The $x$ axis is the *ratio* $(\tau/t_{\mathrm{cor}})$ of the control time $\tau$ and the noise correlation time $t_{\mathrm{cor}}$.

TABLE I. C1 to C4 denote four qubits. The chemical shifts $\nu_i$ and the $J$-coupling $J_{jk}$ are given by the diagonal and off-diagonal elements in (Hz).

| | C1 | C2 | C3 | C4 |
|---|---|---|---|---|
| C1 | 1705.5 | | | |
| C2 | 41.64 | 14 558 | | |
| C3 | 1.46 | 69.72 | 12 330.5 | |
| C4 | 7.04 | 1.18 | 72.36 | 16 764 |

We employ the DFS of the direct product of two two-qubit DFSs given in Sec. III A: $|\tilde{0}\rangle = |01\rangle$ and $|\tilde{1}\rangle = |10\rangle$, where $|0\rangle$ and $|1\rangle$ are eigenstates of $\sigma_z$. The first logical qubit is encoded on C1 and C3, and the second logical qubit is encoded on C2 and C4. In this representation, the two-qubit logical qubits are written as

$$\begin{aligned} |\widetilde{00}\rangle &= |0011\rangle\,, \quad |\widetilde{01}\rangle = |0110\rangle\,, \\ |\widetilde{10}\rangle &= |1001\rangle\,, \quad |\widetilde{11}\rangle = |1100\rangle\,. \end{aligned} \tag{28}$$

Therefore, $H_{\text{eff}} = H_S(t) = H_0 + H_C(t)$ for the same reason discussed in Sec. III A. In this basis, the CNOT gate is expressed as

$$G_{\text{CNOT}} = |\widetilde{00}\rangle\langle\widetilde{00}| + |\widetilde{01}\rangle\langle\widetilde{01}| + |\widetilde{10}\rangle\langle\widetilde{11}| + |\widetilde{11}\rangle\langle\widetilde{10}|\,. \tag{29}$$

The total control time $\tau = 20$ ms and $N = 100$. Set $\lambda = 0.05$ for the DFS condition, and the maximum intensity of the control sequences is set to be $15\pi$ kHz. By optimizing $\{h_\alpha(k)\}$ to maximize $\overline{O}(\{h_\alpha(k)\})$, the algorithm gives the control sequences of $G_{\text{CNOT}}$. The wave forms of the control sequences $h_x(k)$ and $h_y(k)$ are given in Figs. 9(a) and 9(b). To simulate the performance of the CNOT gate, the Hamiltonian with quasistatic environmental noise and control deviation can be written as

$$H(t, \delta, \beta_z) = H_C(t) + (1+\delta)H_C + S_z\beta_z. \tag{30}$$

We calculate the fidelities of the $G_{\text{CNOT}}$ gate searched by our method as shown in Fig. 5(a). In comparison, we also find the control sequences of the $G_{\text{CNOT}}$ by robust GRAPE. The wave forms of control sequences are given in Figs. 9(c) and 9(d). We evaluate the fidelities and depict them in Fig. 5(b). The typical noise $\beta_z$ and the control error $\delta$ has been discussed in Sec. III A. The fidelities of the CNOT gate by our method and robust GRAPE are above 0.991 if $-2$ Hz $\leqslant \beta_z \leqslant 2$ Hz and $-0.5\% \leqslant \delta \leqslant 0.5\%$.

In the simulation with different noises of different correlation times, we employ a classical noise model of pure dephasing as in Eq. (24), where $\beta(t)$ is a Gaussian distributed random variable with $\langle\beta(t)\rangle = 0$ and $\sqrt{\langle\beta(t)^2\rangle} = 2.5$ Hz. The fidelities of the control sequences by our method are not less than 0.99, as shown in Fig. 6. From the results, our method shows better performance against stochastic noise than robust GRAPE.

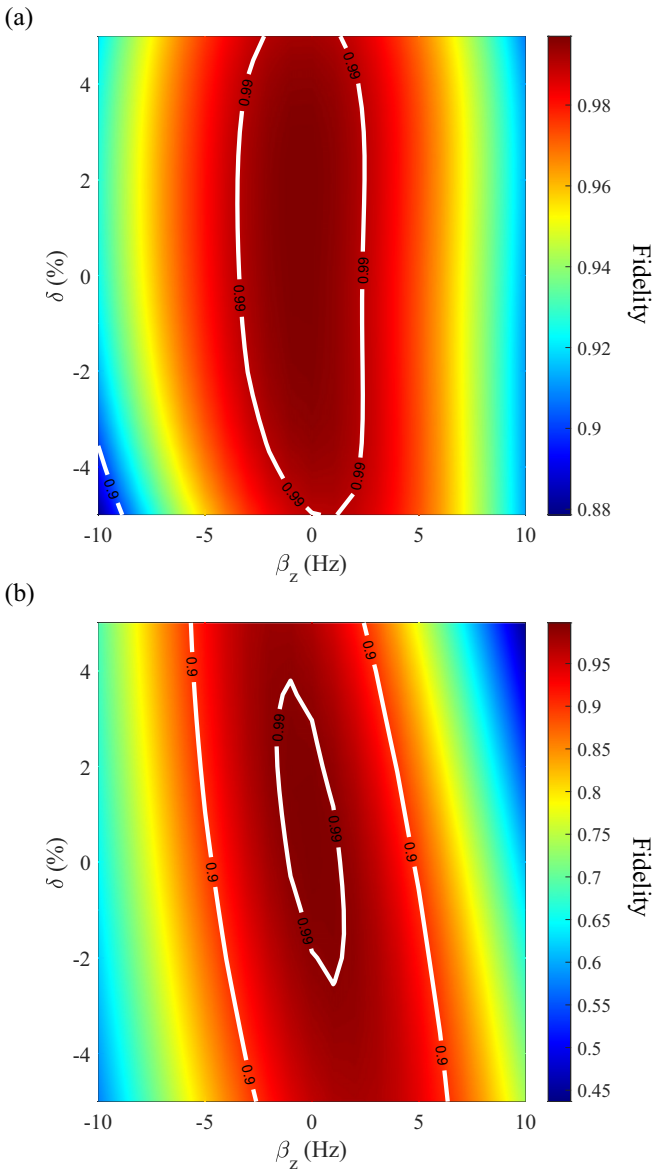


FIG. 5. The fidelities of CNOT gates searched by our method and robust GRAPE, in the presence of quasistatic environmental noise and linear distortion. The $x$ axis represents the environmental noise strength, the $y$ axis represents the control error, and the fidelities of the gates are depicted in the color jets. (a) The fidelities for our method. (b) The fidelities for robust GRAPE.

## IV. CONCLUSION

In summary, we put forward a scheme for optimizing quantum gates combining the idea of DFS with OCT, by generalizing and quantifying the conditions for implementing a quantum gates on DFS. Our method is robust against quasistatic control errors in a natural way. Moreover, our method provides efficiency to find control sequences on systems that the previous method found difficult to handle, by constraining the system to evolve on the DFS for most of the time of the control process but allowing a tiny time to leave from the DFS. As demonstrations of our method, we calculate the control sequences of the NOT, the quantum phase, and the CNOT gates. We also show that our method is better in robustness against stochastic noise than robust GRAPE by numerical simulations.

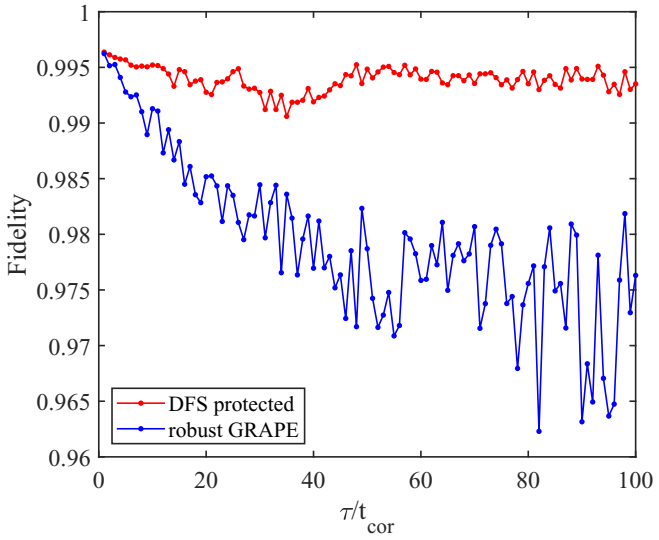


FIG. 6. The fidelities of CNOT gates searched by our method and by robust GRAPE, in a stochastic noise of different correlation times. The red broken line shows our method, and the blue broken line shows robust GRAPE. The $x$ axis is the *ratio* ($\tau/t_{\rm cor}$) of the control time $\tau$ and the noise correlation time $t_{\rm cor}$.

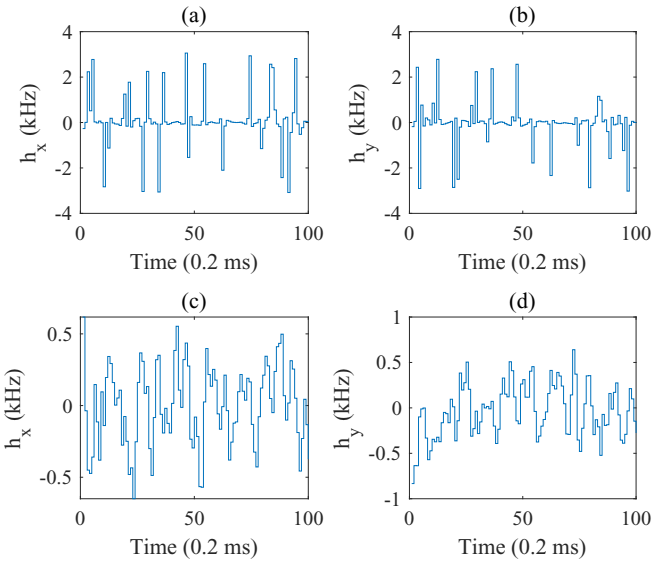


FIG. 7. Control sequences of $G_{\rm NOT}$. (a) and (b) The control sequences of $h_x$ and $h_y$ by our method. (c) and (d) The control sequences of $h_x$ and $h_y$ by robust GRAPE. The total control time $\tau = 20$ ms and is equally divided into 100 steps for both schemes.


## ACKNOWLEDGMENTS

This work is supported by the National Key Research and Development Program of China (Grant No. 2017YFA0303700), the Key R&D Program of Guangdong province (Grant No. 2018B030325002), the Beijing Advanced Innovation Center for Future Chip (ICFC), and Tsinghua University Initiative Scientific Research Program.


## APPENDIX A: METHOD OF CALCULATING INTEGRAL

To compute Eq. (10), we set the following operators:

$$A(t) = \int_0^t U(t)\mathbb{I}_{\rm DFS^\perp}U(t)^\dagger dt, \tag{A1}$$

$$B(t) = \dot{A}(t) = U(t)\mathbb{I}_{\rm DFS^\perp}U(t)^\dagger. \tag{A2}$$

Hence, the derivative of $B(t)$ is

$$\begin{aligned}\dot{B}(t) &= -i\{[H_s + H_C(t)]\cdot B(t) - B(t)\cdot[H_s + H_C(t)]\} \\ &= -i[H_S(t)\cdot B(t) - B(t)\cdot H_S(t)].\end{aligned} \tag{A3}$$

We introduce *Liouville* space ($L$ space) and the *Liouville super operator* described in Refs. [53,54]. We then define a *Liouville super operator* $\mathscr{L}$ in terms of the Hamiltonian operator $[H_S(t) = H_S^\dagger(t)]$:

$$\mathscr{L}(t) = H_S(t)\otimes\mathbb{I} - \mathbb{I}\otimes H_S(t). \tag{A4}$$

The operators $A(t)$ and $B(t)$ in Hilbert space corresponds to vectors in $L$ space such that

$$A(t) \leftrightarrow ||A(t)\rangle\rangle\,, \quad B(t) \leftrightarrow ||B(t)\rangle\rangle\,. \tag{A5}$$

From Eqs. (A1)–(A3), the dynamical equation of $A(t)$ and $B(t)$ can be rephrased in Liouville space as

$$\frac{d}{dt}\begin{pmatrix}||A(t)\rangle\rangle \\ ||B(t)\rangle\rangle\end{pmatrix} = \begin{pmatrix}0 & \mathbb{I}\otimes\mathbb{I} \\ 0 & -i\mathscr{L}(t)\end{pmatrix}\begin{pmatrix}||A(t)\rangle\rangle \\ ||B(t)\rangle\rangle\end{pmatrix}. \tag{A6}$$

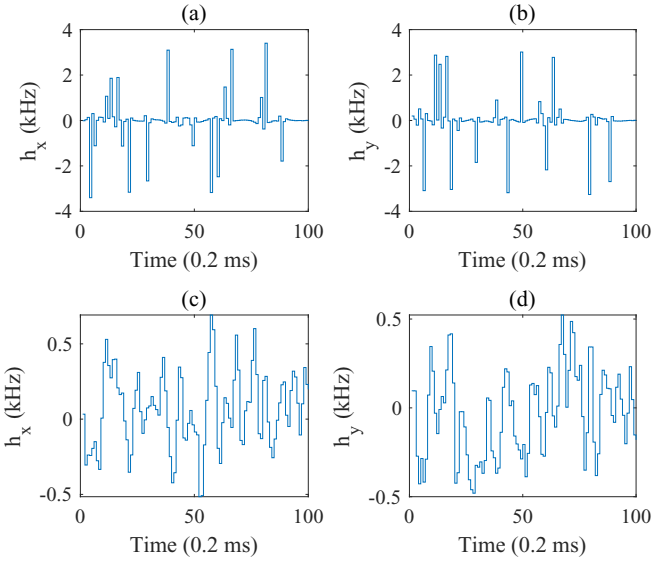


FIG. 8. Control sequences of $G_{\rm phase}$. (a) and (b) The control sequences of $h_x$ and $h_y$ by our method. (c) and (d) The control sequences of $h_x$ and $h_y$ by robust GRAPE. The total control time $\tau = 20$ ms and is equally divided into 100 steps for both schemes.

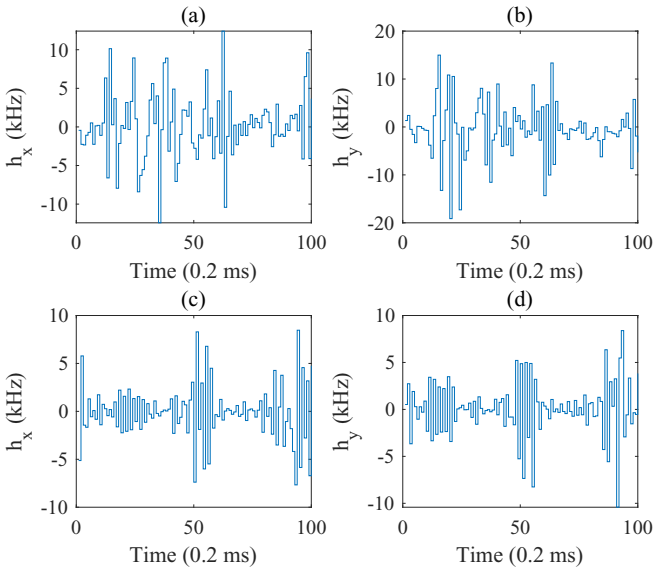


FIG. 9. Control sequences of CNOT gate. (a) and (b) The control sequences of $h_x$ and $h_y$ by our method. (c) and (d) The control sequences of $h_x$ and $h_y$ by robust GRAPE. The total control time $\tau = 20$ ms and is equally divided into 100 for both schemes.

So we can calculate the integrals by

$$\begin{aligned}\begin{pmatrix}||A(\tau)\rangle\rangle\\ ||B(\tau)\rangle\rangle\end{pmatrix} &= \mathcal{T}\exp\left[\int_0^\tau \begin{pmatrix}0 & \mathbb{I}\otimes\mathbb{I}\\ 0 & -i\mathscr{L}(t)\end{pmatrix}dt\right]\begin{pmatrix}||A(0)\rangle\rangle\\ ||B(0)\rangle\rangle\end{pmatrix}\\ &= \prod_k \left\{\exp\left[\begin{pmatrix}0 & \mathbb{I}\otimes\mathbb{I}\\ 0 & -i\mathscr{L}(t_k)\end{pmatrix}\Delta t\right]\right\}\begin{pmatrix}||A(0)\rangle\rangle\\ ||B(0)\rangle\rangle\end{pmatrix}.\end{aligned} \tag{A7}$$

## APPENDIX B: ALGORITHM OF OPTIMIZING OBJECTIVE FUNCTION

The optimization procedure is based on the gradient ascending and is described as the following:

(i) Set the target gate $U_T$, and guess the initial control amplitude $\{h_\alpha(k)\}$.

(ii) Calculate $\overline{O}(\{h_\alpha(k)\})$, and determine whether $\overline{O}(\{h_\alpha(k)\})$ reaches the setting value.

(iii) If yes, stop and return $\{h_\alpha(i)\}$, otherwise compute $\frac{\partial}{\partial h_\alpha(i)}\overline{O}(\{h_i(t)\})$.

(iv) Update to $h_\alpha(k) = h_\alpha(k) + \epsilon\frac{\partial}{\partial h_\alpha(k)}\overline{O}(\{h_\alpha(k)\})$.

(v) Go to step (ii).

The Optimization Toolbox of MATLAB provides another method to work out $\{h_\alpha(k)\}$ by optimizing $\overline{O}(\{h_\alpha(k)\})$.

## APPENDIX C: PROTOCOL FOR ROBUST GRAPE

We present the protocol of GRAPE to design the control sequences of a quantum gate. In the existence of quasistatic environmental noise $\beta_z$ and the control error $\delta$, the real evolution of the system is $U(N,\delta,\beta_z) = \prod_{j=N}^{1}\exp\{-i\frac{\tau}{N}[H_0 + \sum_\alpha(1+\delta)h_\alpha(j)H_\alpha + \beta_z S_z]\}$. To suppress $\beta_z$ and $\delta$, we calculate the average fidelities between the target operation $U_T$ and the evolution $U(N,\delta,\beta_z)$:

$$\overline{O'}(\{h_\alpha(k)\}) = \int d\delta \int d\beta_z p(\delta)p(\beta_z)\frac{|\mathrm{Tr}[U_T^\dagger U(N,\delta,\beta_z)]|^2}{\mathrm{Tr}(\Pi_{\mathrm{DFS}})^2}, \tag{C1}$$

with errors considered in Eq. (23). In practical implementation of the algorithm, the continuous distribution is replaced by discrete distribution. $p(\delta)$ is given in Eq. (22). We take the distribution of the environmental noise $\beta_z$ as

$$p(\beta_z) = \begin{cases}1/3, & \beta_z = 5\text{ Hz},\\ 1/3, & \beta_z = 0\text{ Hz},\\ 1/3, & \beta_z = -5\text{ Hz}.\end{cases} \tag{C2}$$

Then we can use the algorithm described in Appendix B to find the control sequences.

## APPENDIX D: WAVE FORMS OF CONTROL SEQUENCES

The wave forms of the control sequences are presented in Figs. 7, 8, and 9.

[1] P. Benioff, The computer as a physical system: A microscopic quantum mechanical Hamiltonian model of computers as represented by Turing machines, J. Stat. Phys. **22**, 563 (1980).

[2] G.-L. Long, General quantum interference principle and duality computer, Commun. Theor. Phys. (Beijing) **45**, 825 (2006).

[3] D. Suter and G. A. Álvarez, Colloquium: Protecting quantum information against environmental noise, Rev. Modern Phys. **88**, 041001 (2016).

[4] M. H. Levitt, *Spin Dynamics: Basics of Nuclear Magnetic Resonance* (Wiley & Sons, New York, 2013).

[5] I. N. Hincks, C. E. Granade, T. W. Borneman, and D. G. Cory, Controlling Quantum Devices with Nonlinear Hardware, Phys. Rev. Appl. **4**, 024012 (2015).

[6] G. Long, G. Feng, and P. Sprenger, Overcoming synthesizer phase noise in quantum sensing, Quantum Eng. **1**, e27 (2019).

[7] P. Zanardi and F. Rossi, Quantum Information in Semiconductors: Noiseless Encoding in a Quantum-Dot Array, Phys. Rev. Lett. **81**, 4752 (1998).

[8] D. A. Lidar, I. L. Chuang, and K. B. Whaley, Decoherence-Free Subspaces for Quantum Computation, Phys. Rev. Lett. **81**, 2594 (1998).

[9] L.-M. Duan and G.-C. Guo, Reducing decoherence in quantum-computer memory with all quantum bits coupling to the same environment, Phys. Rev. A **57**, 737 (1998).

[10] D. A. Lidar, D. Bacon, and K. B. Whaley, Concatenating Decoherence-Free Subspaces with Quantum Error Correcting Codes, Phys. Rev. Lett. **82**, 4556 (1999).

[11] D. Bacon, J. Kempe, D. A. Lidar, and K. B. Whaley, Universal Fault-Tolerant Quantum Computation on Decoherence-Free Subspaces, Phys. Rev. Lett. **85**, 1758 (2000).

[12] D. P. DiVincenzo, D. Bacon, J. Kempe, G. Burkard, and K. B. Whaley, Universal quantum computation with the exchange interaction, Nature (London) **408**, 339 (2000).

[13] P. G. Kwiat, A. J. Berglund, J. B. Altepeter, and A. G. White, Experimental verification of decoherence-free subspaces, Science **290**, 498 (2000).

[14] E. Knill, R. Laflamme, and L. Viola, Theory of Quantum Error Correction for General Noise, Phys. Rev. Lett. **84**, 2525 (2000).

[15] J. Kempe, D. Bacon, D. A. Lidar, and K. B. Whaley, Theory of decoherence-free fault-tolerant universal quantum computation, Phys. Rev. A **63**, 042307 (2001).

[16] L. Viola, E. M. Fortunato, M. A. Pravia, E. Knill, R. Laflamme, and D. G. Cory, Experimental realization of noiseless subsystems for quantum information processing, Science **293**, 2059 (2001).

[17] D. Kielpinski, V. Meyer, M. Rowe, C. A. Sackett, W. M. Itano, C. Monroe, and D. J. Wineland, A decoherence-free quantum memory using trapped ions, Science **291**, 1013 (2001).

[18] E. M. Fortunato, L. Viola, J. Hodges, G. Teklemariam, and D. G. Cory, Implementation of universal control on a decoherence-free qubit, New J. Phys. **4**, 5 (2002).

[19] M. Mohseni, J. S. Lundeen, K. J. Resch, and A. M. Steinberg, Experimental Application of Decoherence-Free Subspaces in an Optical Quantum-Computing Algorithm, Phys. Rev. Lett. **91**, 187903 (2003).

[20] V. Paulisch, H. Kimble, and A. González-Tudela, Universal quantum computation in waveguide QED using decoherence free subspaces, New J. Phys. **18**, 043041 (2016).

[21] S. Shi, A. Woody, and H. Rabitz, Optimal control of selective vibrational excitation in harmonic linear chain molecules, J. Chem. Phys. **88**, 6870 (1988).

[22] S. J. Glaser, U. Boscain, T. Calarco, C. P. Koch, W. Köckenberger, R. Kosloff, I. Kuprov, B. Luy, S. Schirmer, T. Schulte-Herbrüggen *et al.*, Training Schrödinger's cat: Quantum optimal control, Eur. Phys. J. D **69**, 1 (2015).

[23] N. Khaneja, T. Reiss, C. Kehlet, T. Schulte-Herbrüggen, and S. J. Glaser, Optimal control of coupled spin dynamics: Design of NMR pulse sequences by gradient ascent algorithms, J. Magn. Reson. **172**, 296 (2005).

[24] S. Montangero, T. Calarco, and R. Fazio, Robust Optimal Quantum Gates for Josephson Charge Qubits, Phys. Rev. Lett. **99**, 170501 (2007).

[25] C. A. Ryan, C. Negrevergne, M. Laforest, E. Knill, and R. Laflamme, Liquid-state nuclear magnetic resonance as a testbed for developing quantum control methods, Phys. Rev. A **78**, 012328 (2008).

[26] V. Nebendahl, H. Häffner, and C. F. Roos, Optimal control of entangling operations for trapped-ion quantum computing, Phys. Rev. A **79**, 012312 (2009).

[27] Y. Zhang, C. A. Ryan, R. Laflamme, and J. Baugh, Coherent Control of Two Nuclear Spins Using the Anisotropic Hyperfine Interaction, Phys. Rev. Lett. **107**, 170503 (2011).

[28] D. J. Egger and F. K. Wilhelm, Optimized controlled-Z gates for two superconducting qubits coupled through a resonator, Supercond. Sci. Technol. **27**, 014001 (2013).

[29] G. Waldherr, Y. Wang, S. Zaiser, M. Jamali, T. Schulte-Herbrüggen, H. Abe, T. Ohshima, J. Isoya, J. Du, P. Neumann *et al.*, Quantum error correction in a solid-state hybrid spin register, Nature (London) **506**, 204 (2014).

[30] F. Dolde, V. Bergholm, Y. Wang, I. Jakobi, B. Naydenov, S. Pezzagna, J. Meijer, F. Jelezko, P. Neumann, T. Schulte-Herbrüggen *et al.*, High-fidelity spin entanglement using optimal control, Nat. Commun. **5**, 3371 (2014).

[31] X. Rong, J. Geng, F. Shi, Y. Liu, K. Xu, W. Ma, F. Kong, Z. Jiang, Y. Wu, and J. Du, Experimental fault-tolerant universal quantum gates with solid-state spins under ambient conditions, Nat. Commun. **6**, 8748 (2015).

[32] K. Xu, T. Xie, Z. Li, X. Xu, M. Wang, X. Ye, F. Kong, J. Geng, C. Duan, F. Shi, and J. Du, Experimental Adiabatic Quantum Factorization under Ambient Conditions Based on a Solid-State Single Spin System, Phys. Rev. Lett. **118**, 130504 (2017).

[33] J. Li, X. Yang, X. Peng, and C.-P. Sun, Hybrid Quantum-Classical Approach to Quantum Optimal Control, Phys. Rev. Lett. **118**, 150503 (2017).

[34] K. Li, Eliminating the noise from quantum computing hardware, Quantum Eng. **2**, e28 (2020).

[35] R. I. Karasik, K.-P. Marzlin, B. C. Sanders, and K. B. Whaley, Criteria for dynamically stable decoherence-free subspaces and incoherently generated coherences, Phys. Rev. A **77**, 052301 (2008).

[36] S. Wu, L. Wang, and X. Yi, Time-dependent decoherence-free subspace, J. Phys. A: Math. Theor. **45**, 405305 (2012).

[37] J. Levy, Universal Quantum Computation with Spin-1/2 Pairs and Heisenberg Exchange, Phys. Rev. Lett. **89**, 147902 (2002).

[38] P. E. Spindler, Y. Zhang, B. Endeward, N. Gershernzon, T. E. Skinner, S. J. Glaser, and T. F. Prisner, Shaped optimal control pulses for increased excitation bandwidth in EPR, J. Magn. Reson. **218**, 49 (2012).

[39] T. W. Borneman and D. G. Cory, Bandwidth-limited control and ringdown suppression in high-Q resonators, J. Magn. Reson. **225**, 120 (2012).

[40] G. Jäger and U. Hohenester, Optimal quantum control of Bose-Einstein condensates in magnetic microtraps: Consideration of filter effects, Phys. Rev. A **88**, 035601 (2013).

[41] H. Haas, D. Puzzuoli, F. Zhang, and D. G. Cory, Engineering effective Hamiltonians, New J. Phys. **21**, 103011 (2019).

[42] D. J. Egger and F. K. Wilhelm, Adaptive Hybrid Optimal Quantum Control for Imprecisely Characterized Systems, Phys. Rev. Lett. **112**, 240503 (2014).

[43] Z. Luo, J. Li, Z. Li, L.-Y. Hung, Y. Wan, X. Peng, and J. Du, Experimental preparation of topologically ordered states via adiabatic evolution, Sci. China: Phys., Mech. Astron. **62**, 980311 (2019).

[44] F. Zhang, J. Zhang, P. Gao, and G. Long, Searching nonadiabatic holonomic quantum gates via an optimization algorithm, Phys. Rev. A **100**, 012329 (2019).

[45] G. Lindblad, On the generators of quantum dynamical semigroups, Commun. Math. Phys. **48**, 119 (1976).

[46] B. Schumacher, Sending entanglement through noisy quantum channels, Phys. Rev. A **54**, 2614 (1996).

[47] Y. S. Weinstein, T. F. Havel, J. Emerson, N. Boulant, M. Saraceno, S. Lloyd, and D. G. Cory, Quantum process tomography of the quantum Fourier transform, J. Chem. Phys. **121**, 6117 (2004).

[48] W. G. Unruh, Maintaining coherence in quantum computers, Phys. Rev. A **51**, 992 (1995).

[49] D. Crow and R. Joynt, Classical simulation of quantum dephasing and depolarizing noise, Phys. Rev. A **89**, 042123 (2014).

[50] D. V. Averin, K. Xu, Y. P. Zhong, C. Song, H. Wang, and S. Han, Suppression of Dephasing by Qubit Motion in Superconducting Circuits, Phys. Rev. Lett. **116**, 010501 (2016).

[51] P. Solinas, P. Zanardi, and N. Zanghì, Robustness of non-Abelian holonomic quantum gates against parametric noise, Phys. Rev. A **70**, 042316 (2004).

[52] X. Kong, T. Xin, S.-J. Wei, B. Wang, Y. Wang, K. Li, and G.-L. Long, Demonstration of multiparty quantum clock synchronization, Quantum Inf. Process. **17**, 1 (2018).

[53] B. Dalton, Liouville space theory of sequential quantum processes. I. general theory, J. Phys. A: Math. Gen. **15**, 2157 (1982).

[54] S. Barnett and B. Dalton, Liouville space description of thermofields and their generalisations, J. Phys. A: Math. Gen. **20**, 411 (1987).